Methyl *t*-Butyl Ether and Methyl Trimethylsilyl Ether Ions Dissociate near Their Ionization Thresholds: A TPES, TPEPICO, RRKM, and G3 Investigation

Emma E. Rennie,[†,#] Louise Cooper,[‡] Larisa G. Shpinkova,[§] David M. P. Holland,[⊥] David A. Shaw,[⊥] Martyn F. Guest,[¶] and Paul M. Mayer*[,†]

Department of Chemistry, University of Ottawa, 10 Marie-Curie, Ottawa, Canada K1N 6N5, Department of Chemistry, Heriot-Watt University, Riccarton, Edinburgh EH14 4AS, U.K., Department of Nuclear Spectroscopy Methods, Institute of Nuclear Physics, Moscow State University, Moscow 119899, Russia, Daresbury Laboratory, Daresbury, Warrington, Cheshire WA4 4AD, U.K., and Advanced Research Computing, Cardiff University, Redwood Building, King Edward VII Avenue, Cardiff CF10 3NB, Wales, U.K.

Received: February 3, 2009; Revised Manuscript Received: March 31, 2009

The threshold photoelectron spectra and threshold photoelectron photoion coincidence (TPEPICO) mass spectra of methyl *t*-butyl ether, $(CH_3)_3COCH_3$ (MTBE), and methyl trimethylsilyl ether, $(CH_3)_3SiOCH_3$ (MTMSE), have been measured using synchrotron radiation. The effect of silicon substitution on the unimolecular dissociation processes and the threshold photoelectron spectrum has been investigated. Both molecular ions dissociate at low internal energies. For ionized MTBE, the parent ion is no longer observed at an internal energy of only 0.2 eV. For this reason, it was not possible to fit the TPEPICO data to extract reliable thermochemical information. G3 level calculations place the molecular ion 5 kJ mol^{-1} above the lowest-energy dissociation products, $(CH_3)_2COCH_3^+ + {}^{\bullet}CH_3$, suggesting the participation of an isomer, potentially the distonic ion ${}^{\bullet}CH_2(CH_3)_2CO^+(H)CH_3$, in the dissociation. However, the calculations are not considered accurate enough to reliably determine the role this isomer plays, if any. RRKM modeling of the threshold region of the TPEPICO breakdown curves for ionized MTMSE leads to an E_0 for methyl loss of 63 ± 2 kJ mol^{-1}, in good agreement with the G3 value of 66 kJ mol^{-1}. The resulting $\Delta_f H_0$ for $(CH_3)_2SiOCH_3^+$ of 384 ± 10 kJ mol^{-1} ($\Delta_f H_{298}$ = 361 ± 10 kJ mol^{-1}) is 28 kJ mol^{-1} lower than the G3 value of 412 kJ mol^{-1} due to the G3 $\Delta_f H_0$ for neutral MTMSE being 16 kJ mol^{-1} higher than the previously reported value and the fact that the experimental IE_a is 6 kJ mol^{-1} lower than the G3 estimate. Appearance energy values for higher-energy fragmentation channels up to 36 (for MTBE) and 32 eV (for MTMSE) are reported and compared to literature values. An investigation of fragment ion peak broadening at high internal energy indicated that the two doubly charged molecular ions are not stable on the microsecond time scale. Each was found to dissociate into two singly charged ions along one or more neutral species.

Introduction

Methyl tertiary-butyl ether (MTBE) with the chemical structure $(CH_3)_3COCH_3$ is produced in very large quantities (over 200 000 barrels per day in the U.S. in 1999) and is almost exclusively used as a fuel additive in motor gasoline at concentrations up to 15% by volume. This increases the oxygen content, enhances the efficiency in internal combustion engines, and reduces the emissions of carbon oxide, benzene, and other organic compounds from motor vehicles.[1,2] At room temperature, MTBE is a volatile, flammable, and colorless liquid with a high water solubility that, combined with its high vapor pressure and widespread use in fuels, causes additional pollution of urban stormwater, groundwater, and surface water. Hence, most of the recent literature on MBTE deals with its potential impact on the environment and human health.[1,2] Bhat et al.[3] used density functional theory to study the thermodynamics and kinetics of MTBE degradation. They investigated the unimolecular decomposition of neutral and protonated MTBE to produce $(CH_3)_2C{=}CH_2 + CH_3OH$ and $(CH_3)_2C{=}CH_2 + CH_3OH_2^+$, respectively. The authors concluded that unimolecular decomposition is not a significant degradation mechanism in vacuo or in aqueous solution at ambient temperatures. However, this study did not include the unimolecular dissociation reactions of the radical cation. Any neutral MTBE which escapes the troposphere, into the mesosphere and beyond, will absorb sufficiently energetic photons to produce ionized MTBE, and thus, the low-energy dissociations of ionized MTBE should be considered as a significant decomposition mechanism in vacuo. Bissonnette et al.[4] obtained the electron ionization (EI), metastable ion (MIKES), and collision-induced dissociation (CID) mass spectra of MTBE. They reported a base peak in the EI mass spectrum of *m*/*z* 73 ($(CH_3)_2COCH_3^+$) resulting from the loss of a methyl group ($CH_3^{\bullet}$); this peak was also the major peak in the MIKES mass spectrum of ionized MTBE along with a minor peak with *m*/*z* 72 due to loss of methane (CH_4). Isotopic labeling[4] was used to show that H/D mixing did not occur before fragmentation as all peaks in the mass spectrum cleanly shifted upon deuteration. An appearance energy (measured using electrons of low-energy resolution) of 9.52 ± 0.05 eV was measured for both channels, and it was suggested that the

* To whom correspondence should be addressed. E-mail: pmmayer@uottawa.ca. Fax (613) 562-5170.
† University of Ottawa.
‡ Heriot-Watt University.
§ Moscow State University.
⊥ Daresbury Laboratory.
¶ Cardiff University.
# Present address: Varian, Inc., 2700 Mitchell Drive, Walnut Creek, CA 94598.

10.1021/jp900991p CCC: $40.75
Published on Web 04/23/2009

appearance energies lie so close to their measured ionization threshold of 9.24 eV as to preclude the possibility of the reactions being metastable, unless a (deep) nearby potential well can be accessed by the molecular ion. Beveridge et al.[5] investigated the possibility of the unimolecular dissociation of ionized MTBE occurring via an ion−neutral complex as suggested by Bissonnette et al.[4]

Methyl trimethylsilyl ether (MTMSE), a silicated analogue of MTBE, has the structure $(CH_3)_3SiOCH_3$. There have been few gas-phase studies of this molecule; Hess et al.[6] used electron ionization to study the ionization and dissociation of trimethylsilanes, and Orlando et al.[7] investigated the ion chemistry and thermochemistry of several trimethylsilyl compounds. Mölder et al.[8] measured the photoelectron spectrum of MTMSE and assigned molecular orbital characters with the aid of semiempirical CNDO/2 calculations. Sutherland et al.[9] have measured the vibrational splitting in the Silicon 2p core-level photoelectron spectra of MTMSE.

In this study, the comparison between MTBE and MTMSE has allowed the effect of silicon substitution on ion stability and fragmentation mechanisms to be investigated. We have recorded the threshold photoelectron spectra of MTBE and MTMSE from threshold to 24 and 30 eV, respectively, using synchrotron radiation. The observed bands have been assigned through comparison with vertical ionization energies and intensities computed using the outer valence Green's function approach. In addition, threshold photoelectron photoion coincidence (TPEPICO) mass spectra have been measured from threshold to 36 (MTBE) and 32 (MTMSE) eV. These spectra have allowed dissociation thresholds for fragment ions to be derived, and the results are compared with previous values where possible. Kinetic modeling of the threshold region for $CH_3^{\bullet}$ loss from ionized MTMSE leads to a new 0 K activation energy for the processes and, consequently, to a new heat of formation ($\Delta_f H$) for $(CH_3)_2SiOCH_3^+$.

TABLE 1: Comparison of G3 and Experimental Relative Energies for the MBTE and MTMSE Ions and Their Respective Fragmentation Products

	relative G3 energies (0 K, kJ mol^{-1})	experimental relative enthalpies (kJ mol^{-1})[a]
MBTE		
$(CH_3)_3COCH_3$ (C_1)	−919	−891
$(CH_3)_3COCH_3^{+\bullet}$	0	0
$(CH_3)_3COCH_3^{+\bullet}$−vertical ion	18	
$(CH_3)_2(CH_2)CO(H)CH_3^{+\bullet}$− distonic ion	−20	
$(CH_3)_3CO(H)CH_2^{+\bullet}$	−3	
$(CH_3)_2COCH_3^+ + CH_3^{\bullet}$	−5	16
$(CH_3)(CH_2)CO(H)CH_3^+ + CH_3^{\bullet}$	110	
$(CH_3)_3COCH_3^{2+}$(singlet)	1175	
$(CH_3)_3COCH_3^{2+\bullet\bullet}$(triplet)	1522	
MTMSE		
$(CH_3)_3SiOCH_3$ (C_1)	−904	−927
$(CH_3)_3SiOCH_3^{+\bullet}$	0	0
$(CH_3)_3SiOCH_3^{+\bullet}$−vertical ion	67	
$(CH_3)_2(CH_2)SiO(H)CH_3^{+\bullet}$− distonic ion	−6	
$(CH_3)_3SiO(H)CH_2^{+\bullet}$	13	
$(CH_3)_2SiOCH_3^+ + CH_3^{\bullet}$	66	63 ± 2[b]
$(CH_3)(CH_2)SiO(H)CH_3^+ + CH_3^{\bullet}$	282	
$(CH_3)_3SiOCH_3^{2+}$(singlet)	1159	
$(CH_3)_3SiOCH_3^{2+\bullet\bullet}$(triplet)	1469	

[a] Experimental values are based on $\Delta_f H$ values taken from ref 17, unless otherwise indicated. [b] The present result is from RRKM fitting of the TPEPICO breakdown curves.

Experimental Details Section

The pulsed TPEPICO spectrometer,[10] in which the dissociation, kinetic, and threshold photoelectron studies were performed, and the 5 m normal incidence monochromator,[11] attached to the Daresbury Laboratory synchrotron radiation source, have been described in detail previously. The coincidence spectrometer employs a pulsed extraction technique,[12] the principal advantage of which is that threshold electrons can be detected with a high-energy resolution, while also allowing the associated ions to be collected with a high mass resolution. In the present arrangement,[10] a very low electric field is applied initially across the interaction region to extract threshold electrons. The detection of the electron triggers the application of a high-voltage (∼1 kV) pulse across the interaction region to draw the ion toward the drift tube and initiates the TOF measurement. The time between the arrival of the electron and that of the associated ion is measured electronically, with the summation of many events producing a TOF spectrum. One of the advantages of the pulsed extraction technique is that breakdown curves can be measured as a function of ion residence time in the interaction region by varying the delay between the detection of the threshold electron and the application of the ion drawout field. The residence time is defined as the period between the creation of the electron−ion pair and the application of the pulse and is given by the transit time of the electron added to the electronic signal processing time. With the present apparatus, the minimum residence time has been measured as 1.116 ± 0.050 μs using the experimental procedure described in Holland et al.[10] The breakdown curves in the threshold energy region were measured for three residence times by adding additional electronic delays of 2 μs. That is, the actual residence times were 1.116, 3.116, and 5.116 μs.

Threshold photoelectron spectra were recorded in the binding energy range from ∼9 to 24 (MTBE) and 30 (MTMSE) eV using only the electron detection part of the coincidence spectrometer. The spectra were normalized to variations in the incident photon intensity using the signal from a photomultiplier which monitored the monochromated radiation after it impinged upon a sodium salicylate coated screen. The threshold photoelectron spectra were measured at a photon resolution of 0.1 nm fwhm (∼18 meV at $h\nu = 15$ eV). Lithium fluoride or indium filters could be inserted into the photon beam exiting the monochromator to help suppress higher-order radiation. The binding energy scale was calibrated by recording a threshold photoelectron spectrum of a gas mixture comprised of MTBE (or MTMSE), argon, and xenon.

Computational Procedures Section

Standard ab initio molecular orbital calculations[13] were performed using the Gaussian 98[14] suite of programs. Geometries for the ionic and neutral species were optimized, and harmonic vibrational frequencies were calculated at the MP2/6-31+G(d) level of theory. The resulting MP2/6-31+G(d) geometries and zero-point energies (ZPEs) (scaled by 0.967)[15] were then used to obtain G3[16] total energies. These energies are listed in Table S1 of Supporting Information. The relative energies, given in relation to the relevant molecular ion, are summarized in Table 1, along with the relevant dissociation energies. In our thermochemical estimations, the recommended $\Delta_f H$ values tabulated in the NIST Chemistry Database[17] and by Lias et al.[18] have been used unless stated otherwise. The G3 total energies were translated to enthalpies of formation ac-

TABLE 2: Experimental and OVGF Vertical Ionization Energies and Charge Distribution Analyses of MTBE

	ionization energy (eV)		orbital character (% atomic population)					
			$(CH_3)_3-$		$-C-$	$-O-$	$-(CH_3)$	
orbital	OVGF	experiment	C	H	C	O	C	H
1	25.73		35.6	14.4	35.8	8.0	4.5	1.6
2	23.06		35.1	24.4	14.5	7.1	10.6	8.3
3	22.84		51.1	33.8	14.2	0.6	0.1	0.2
4	22.32		18.9	13.8	6.3	9.8	29.3	22.0
5	18.44	18.24	27.7	21.4	16.3	19.0	9.7	6.0
6	16.33	16.31	29.3	20.4	18.3	13.5	11.0	7.5
7	15.71	15.74	19.2	12.0	9.0	30.2	17.6	12.0
8	15.64	23.1	15.8	13.1	22.9	16.5	8.6	
9	15.06		36.1	26.5	7.1	1.6	14.8	13.9
10	14.50		38.9	31.8	2.3	12.0	9.3	5.7
11	13.99		31.3	29.9	3.5	5.9	16.1	13.4
12	13.53		44.2	41.4	0.9	0.5	7.2	5.8
13	13.24		41.6	42.1	1.0	7.9	5.2	2.2
14	13.06		49.2	50.0	0.0	0.6	0.4	0.1
15	12.12	11.94	36.9	25.4	13.1	10.4	5.9	8.2
16	12.11	23.6	16.1	15.7	21.2	10.9	12.5	
17	10.88	10.89	30.2	12.5	17.2	27.5	6.5	6.0
18	9.63	9.59	18.5	0.5	8.6	51.1	5.2	11.2

TABLE 3: Experimental and OVGF Vertical Ionization Energies and Charge Distribution Analyses of MTMSE

	ionization energy (eV)		orbital character (% atomic population)					
			$(CH_3)_3-$		$-Si-$	$-O-$	$-(CH_3)$	
orbital	OVGF	experiment	C	H	Si	O	C	H
	23.39		52.4	28.3	11.0	2.9	3.4	2.0
2	22.57		39.9	27.0	8.0	5.4	11.3	8.4
3	22.39		54.6	37.3	7.9	0.1	0.0	0.0
4	22.42		18.4	12.9	4.4	11.4	29.8	23.1
5	16.91	16.81	14.4	5.7	14.4	36.6	19.0	9.9
6	15.36	15.48	3.3	2.1	3.0	31.3	34.2	26.2
7	15.22	7.2	4.4	5.4	31.3	32.1	19.6	
8	14.78		42.7	25.8	17.3	7.9	4.4	2.0
9	14.29		48.6	42.8	5.2	0.2	1.5	1.8
10	14.22		48.0	43.9	3.7	1.6	1.7	1.1
11	13.78		40.9	33.6	6.3	4.3	8.3	6.5
12	13.68		48.8	45.6	1.0	0.1	2.5	2.0
13	13.55		45.5	41.5	2.7	6.7	2.8	0.7
14	13.46		52.0	47.8	0.0	0.0	0.1	0.0
15	11.48	11.54	12.1	4.7	11.7	40.2	13.0	18.2
16	11.39	19.3	8.1	11.8	34.3	10.7	15.7	
17	10.38	10.48	53.3	10.9	21.5	10.9	1.8	1.6
18	9.87	9.88	44.1	7.4	15.0	26.2	2.3	5.1

cording to the atomization procedure described by Nicolaides et al.[19] (Table S2 in Supporting Information).

Vertical ionization energies and their relative spectral intensities (pole strengths) of MTBE and MTMSE were obtained using the outer valence Green's function (OVGF) approach.[20] The calculations employed the GAMESS-UK[21,22] suite of programs, with a variety of basis sets. For consistency, the geometries of both species were fully optimized at the MP2 level using both cc-pVTZ and cc-pVDZ basis sets.[23−26] The OVGF calculations for both species were performed at the cc-pVTZ optimized equilibrium geometries of C_1 symmetry using the cc-pVDZ basis set. Ten inner-shell orbitals, corresponding to the 1s orbitals of C and O and the 1s, 2s, and 2p orbitals of Si, were frozen in the OVGF calculation on MTMSE. Six such orbitals—the 1s functions on each C and O—were frozen in the calculation on MTBE. The results are listed in Tables 2 and 3, together with charge distribution analyses derived from a Mulliken population analysis of the single configuration (Hartree−Fock SCF) wave function generated at the same geometry used in the OVGF calculations.

The lowest-energy dissociation channels were modeled with the standard RRKM rate expression

$$k(E) = \frac{\sigma}{h}\frac{N^{\ddagger}(E - E_0)}{\rho(E)} \quad (1)$$

where $k(E)$ is the unimolecular rate constant at an ion internal energy, E, σ is the reaction degeneracy or symmetry number, h is Planck's constant, E_0 is the 0 K activation energy, $\rho(E)$ is the reactant ion rovibrational density of states, and $N^{\ddagger}(E - E_0)$ is the transition-state rovibrational sum of states.[27,28] The density and sum of states calculations employed the direct count algorithm of Beyer and Swinehart.[29] It is necessary to know, or to guess, the barrier height or activation energy and the vibrational frequencies of both the reactant ion and the transition state. The reactant ion frequencies were taken from the MP2/6-31+G(d) geometry. Initial transition-state frequencies were chosen to be the same as those for the reactant ion, with a C−C stretch removed to approximate the reaction coordinate. The next step in the analysis[30−32] involves convoluting the theoretical $k(E)$ curves with the parent ion thermal (rotational and vibra-

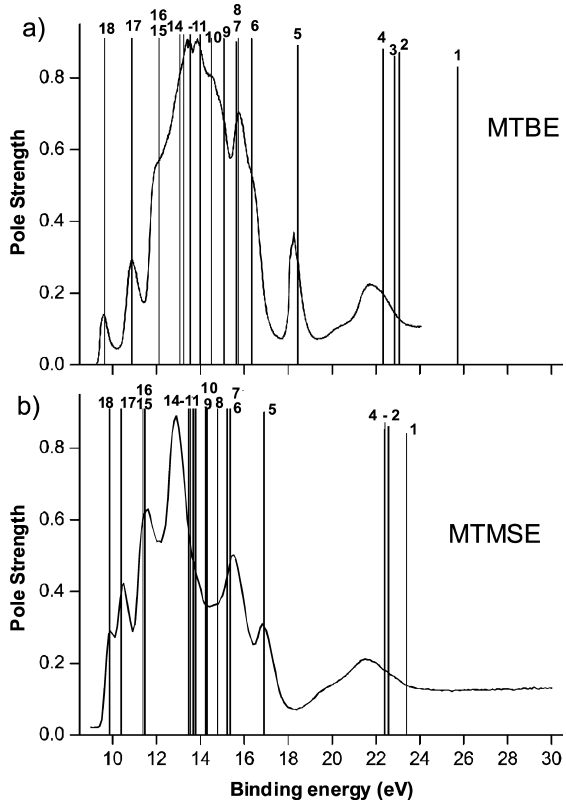

Figure 1. (a) The threshold photoelectron spectrum of MTBE together with the theoretical results (Table 2). The height of the bar is proportional to the calculated relative spectral intensity (pole strength). (b) The threshold photoelectron spectrum of MTMSE together with the theoretical results (Table 3). The height of the bar is proportional to the calculated relative spectral intensity (pole strength).

tional) energy, the monochromator band-pass function (photon resolution ~8 meV), and the threshold electron analyzer transmission function (width of ~9 meV full width at half-maximium) derived from a threshold electron spectrum obtained from the photoionization of krypton in the region of the $^2P_{1/2}$ ionization limit under the conditions used in the TPEPICO measurements. The activation energy, E_0, and the transition state's vibrational frequencies were varied in the RRKM calculation until a satisfactory fit to the experimental breakdown curves, obtained at ion residence times of 1.116, 3.116, and 5.116 μs, was found.

Results and Discussion

Threshold Photoelectron Spectra of MTBE and MTMSE. The threshold photoelectron spectra of MTBE and MTMSE are plotted in Figure 1, together with the OVGF ionization energies and relative spectral intensities. In each molecule, the calculations indicate that the single-particle model of ionization[33] holds reasonably well for 18 of the 19 valence orbitals. The theoretical results for the innermost valence orbital, where the single-particle model of ionization breaks down, are not included in Tables 2 and 3. The observed vertical ionization energies, obtained through inspection of the experimental spectra, are also listed in the tables, for those orbitals where a distinct feature is discernible. No attempt was made to fit the spectra because the vibrational envelope associated with a specific orbital is unknown and is likely to vary from orbital to orbital. Furthermore, many of the vibrational envelopes overlap one another and are affected by autoionization. The OVGF ionization energies, particularly those for MTBE, are in good agreement with the measured values, thereby enabling structure in the experimental spectra to be correlated with ionization from specific molecular orbitals.

In MTBE, the photoelectron bands with maxima at 9.59 and 10.89 eV evidently correspond to ionization from the two outermost orbitals (18,17), and the shoulder at 11.94 eV is associated with the next two orbitals (16,15), which are predicted to have similar ionization energies (Table 2). The peak at 15.74 eV may be attributed to the two orbitals (8,7) with calculated ionization energies of 15.64 and 15.71 eV, and the shoulder observed at higher energy (16.31 eV) coincides with the next orbital (6), whose theoretical energy is 16.33 eV. The well-separated peak occurring at 18.24 eV arises from the orbital (5) predicted at 18.44 eV, and in the inner valence region, the theoretical results indicate that the broad feature appearing at around 22 eV should be associated with three close-lying orbitals.

Inspection of the threshold photoelectron spectrum of MTBE gives $IE_a = 9.25 \pm 0.05$ eV and $IE_v = 9.59$ eV. These results are in excellent agreement with those of 9.24[4] and 9.31[34] eV for IE_a and 9.48[35] and 9.41[36] eV for IE_v. The difference between the vertical and adiabatic IE values stems from the geometry of the ground-state ion. Most species with a *t*-butyl moiety exhibit in their molecular radical cations a long $(CH_3)_2C-CH_3$ bond. In the case of TBME, this bond length is 1.79 Å, as compared to the other two bonds at 1.51 Å. In neutral TBME, all three bonds are ~1.53 Å. The calculated G3 IE_a of 9.53 eV (Table 1) is significantly higher than the experimental result. In fact, the measured IE_a tends to be in better agreement with the G3 energy difference of 9.33 eV (Table 1) between neutral MTBE and the ground state of the distonic ion $^{\bullet}CH_2(CH_3)_2CO^+(H)CH_3$. At the G3 level of theory, the MTBE ion resides 5 kJ mol^{-1} above the methyl loss products (Table 1). The participation of a deeper, adjacent well on the potential energy surface is consistent with the arguments by Bissonette et al.[4] that such a well would be necessary to make this dissociation occur on the metastable time frame. Computationally, however, the ion is bound in the absence of the ZPE correction by 24 kJ mol^{-1}, and therefore, it is impossible, with the presently applied theory, to conclude the nature of the ion formed when neutral MTBE is ionized.

A broadly similar interpretation can be given for the threshold photoelectron spectrum of MTMSE. The peaks with maxima at 9.88, 10.48, and 11.54 eV correspond to ionization from the orbitals (18−15) calculated at 9.87, 10.38, 11.39, and 11.48 eV, respectively. Likewise, the peaks observed at 15.48 and 16.81 eV are associated with the orbitals (7−5) predicted at 15.22, 15.36, and 16.91 eV, respectively. In the inner valence region, the feature with a maximum at ~21.6 eV lies slightly lower in energy than the theoretical results, as was also found for the corresponding structure in MTBE.

From the threshold photoelectron spectrum of MTMSE, we obtain $IE_a = 9.31 \pm 0.05$ eV and $IE_v = 9.88$ eV, in accord with previous experimental values of 9.85[8] and 9.79 ± 0.04[6] eV for IE_v and the present G3 IE_a of 9.37 eV. In this case, the G3 calculations predict the MTMSE ion to be bound with respect to dissociation by 66 kJ mol^{-1} (Table 1). As in TBME, the large difference between IE_a and IE_v can be traced to the $(CH_3)_2Si-CH_3$ bond. In the ion, one of these bonds is 2.29 Å, as compared to the other two bonds at 1.89 Å. In neutral MTMSE, all three bonds are ~1.88 Å.

The He(I) excited photoelectron spectrum of MTMSE has been recorded by Mölder et al.[8] and exhibits two structureless bands, with vertical ionization energies of 9.85 and 10.64 eV,

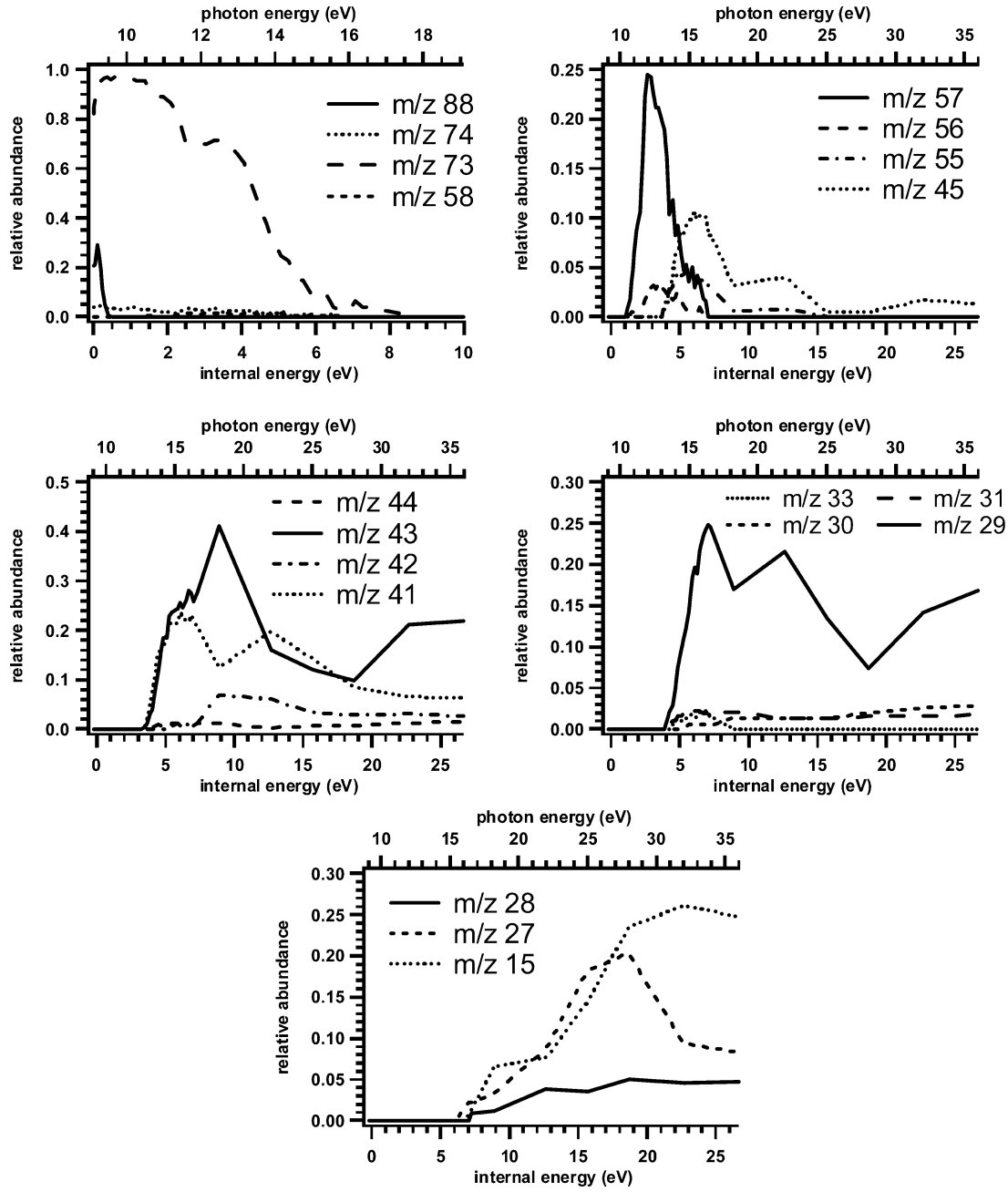

Figure 2. Breakdown diagrams for MTBE derived from the TOF mass spectra recorded at an ion source residence time of 1.116 μs.

which evidently correlate with those at 9.88 and 10.48 eV in the threshold photoelectron spectrum (Figure 1b). However, at higher energies, the He(I) excited and the threshold photoelectron spectra differ. The intensity in the He(I) excited spectrum decreases to approximately 0 at 11.5 eV before increasing again to form a broad band between ~12 and 16 eV. This band does not resemble the corresponding features in the threshold photoelectron spectrum possibly due to the effect of resonant ionization on the latter spectrum. It is also noticeable that the threshold photoelectron yield remains finite across the entire excitation range, including the Franck−Condon gap at around 11.5 eV.

The signal in a conventional He(I)-excited electron energy resolved spectrum arises predominantly through direct photoionization. In contrast, resonant autoionization, an indirect two-step process, often influences threshold photoelectron spectra and can affect both the band profile and the relative intensity. The differences apparent in the He(I) excited and threshold photoelectron spectra of MTMSE are typical of those observed in small polyatomic molecules.[37,38] Experimentally, it has been found that the relative intensities of photoelectron bands associated with weakly bound orbitals tend to be greater in conventional spectra than those in threshold photoelectron spectra, whereas the converse holds for the more tightly bound orbitals. The enhancement in the latter bands can be attributed to resonant autoionization from numerous superexcited (Rydberg or valence) states.

As threshold photoelectron spectra are strongly affected by autoionization, the structure in such spectra often resembles that in the corresponding ion yield curves.[39,40] The parent ion yield of $(CH_3)_3COCD_3$ has been measured between threshold and 12.5 eV by Chambreau et al.[34] and exhibits maxima at 9.5, 10.1, 10.8, and 12.0 eV. The peaks at 9.59, 10.89, and 11.94 eV in the threshold photoelectron spectrum of MTBE clearly correlate with three of the ion yield maxima.

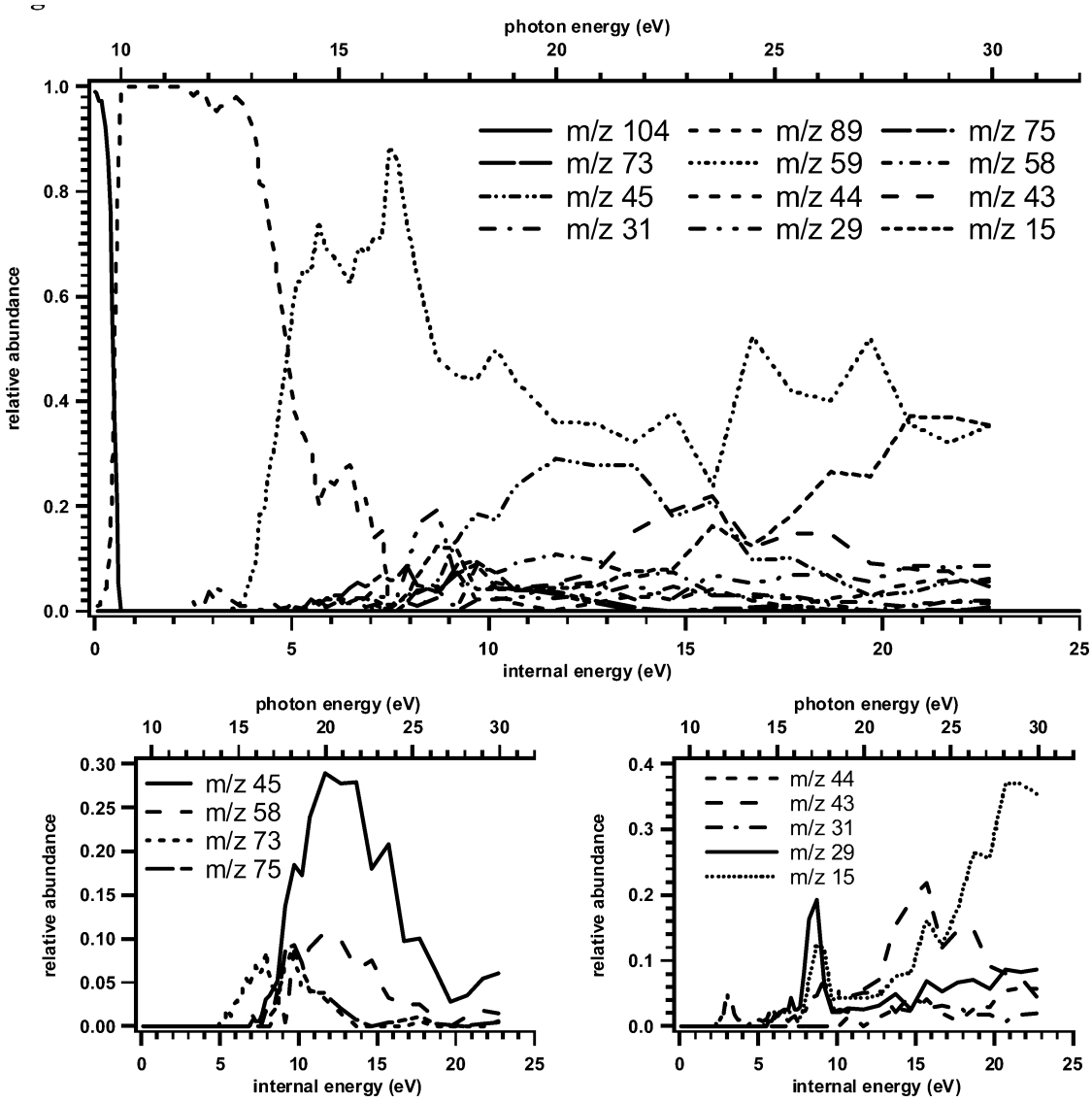

Figure 3. Breakdown diagram for MTMSE derived from the TOF spectra recorded at an ion source residence time of 1.116 μs.

The charge distribution analyses given in Tables 2 and 3 may be used to characterize the molecular orbitals in terms of atomic populations. In molecules of low symmetry, such as the C_1 symmetry applicable to MTBE and MTMSE, it is often useful to group together individual contributions into small molecular species relevant to that particular molecule. The charge distributions listed in Tables 2 and 3 are presented in this manner. Taking MTBE as an example, the results show that while there is some contribution from the $(CH_3)_3$ (19%) and CH_3 (16%) components, the electron density for the outermost orbital is concentrated on the oxygen atom (51%), consistent with previous predictions that this orbital is essentially a nonbonding atomic orbital located on the oxygen atom.[5,8] There then follows a group of orbitals, calculated to lie in the binding energy range of ~10.5 to 14.5 eV, which have only small contributions from the single CH_3 species but significant contributions from the C 2p and H 1s orbitals on the $(CH_3)_3$ component. Some of these orbitals also possess substantial O 2p character. For the more tightly bound orbitals, the electron density is distributed over the whole molecule and is dominated by the C 2s atomic contributions. The innermost valence orbital, not included in Tables 2 and 3, is essentially an O 2s atomic orbital.

The character of the orbitals in MTMSE are similar to those in MTBE, the principal difference being that the outermost orbital cannot be regarded simply as a nonbonding oxygen atomic orbital, contrary to earlier predictions.[8] In contrast to MTBE, where the orbital featured 51% oxygen character, the dominant contribution in MTMSE arises from the $(CH_3)_3$ component (52%), with the oxygen character reduced to 26%.

TPEPICO TOF Mass Spectra. Coincidence spectra were collected in the photon energy range of 9.1−36 eV for MTBE and 9.4−32 eV for MTMSE. In both cases, even just above the ionization threshold, the molecular ion was always accompanied by one or more fragment ions in the TOF spectra. Breakdown curves for all observed ions are presented in Figures 2 and 3 for MTBE and MTMSE, respectively. Appearance energies (AEs) of the fragment ions, derived from the TOF spectra, are listed along with literature values in Tables 4 and 5. The large uncertainty quoted with our AE is due solely to the energy spacing at which the TOF spectra were measured. The observed low-energy dissociations produce the $(CH_3)_2COCH_3^+$ (*m/z* 73) and $(CH_3)_2SiOCH_3^+$ (*m/z* 89) ions associated with the loss of a methyl radical. The ions appear at 9.10 ± 0.05 (MTBE) and 9.41 ± 0.05 eV (MTMSE), lower than the earlier literature values (see Table 4 and 5) due to smearing out of the breakdown diagrams near the dissociation threshold from experimental parameters, in particular, the electron transmission function. This has been reported previously

TABLE 4: Fragment Ion Appearance Energies for MTBE

		AE (298 K, eV)	
m/z	fragment ion	this work	literature
73	$(CH_3)_2COCH_3^+$	9.10 ± 0.05[a]	9.52 ± 0.05,[4] 9.46[43]
57	$(CH_3)_3C^+$	10.5 ± 0.1	
56	$C_4H_8^+/C_3H_5O^+$	10.6 ± 0.1	
58	$CH_3COCH_3^{+\bullet}$	10.7 ± 0.1	
43	$C_3H_7^+/COCH_3^+$	12.8 ± 0.2	
41	$C_3H_5^+/C_2HO^+$	13.0 ± 0.2	
44	$C_3H_8^+/C_2H_4O^+$	13.0 ± 0.2	
45	$C_3H_9^+/C_2H_5O^+$	13.2 ± 0.2	
55	$C_4H_7^+/C_3H_4O^+$	13.2 ± 0.2	
29	$C_2H_5^+/CHO^+$	13.4 ± 0.2	
31	CH_3O^+	13.4 ± 0.2	
33	CH_5O^+	13.8 ± 0.2	
30	$C_2H_6^{+\bullet}/CH_2O$	14.8 ± 0.2	
42	$C_3H_6^+/CH_2CO^{+\bullet}$	14.8 ± 0.2	
27	$C_2H_3^+$	15.8 ± 0.2	
15	CH_3^+	16.4 ± 0.2	
39	$C_3H_3^+$	16.4 ± 0.2	
28	$C_2H_4^+/CO$	16.6 ± 0.2	
40	$C_3H_4^+/C_2O^+$	18.2 ± 2	

[a] This value is greatly affected by experimental smearing of the breakdown curves near the ionization threshold.

TABLE 5: Fragment Ion Appearance Energies for MTMSE

		AE (298 K, eV)	
m/z	fragment ion	this work	literature
89	$C_3H_9SiO^+$	9.40 ± 0.05[a]	10.25 ± 0.05[6]
31	$C_2H_7^+/H_3Si^+/CH_3O^+$	11.7 ± 0.1	
59	$C_4H_{11}^+/CH_3SiO^+/C_2H_7Si^+/C_3H_7O^+$	12.8 ± 0.1	
73	$C_2H_5SiO^+/C_3H_9Si^+/C_4H_9O^+$	14.4 ± 0.2	12.43 ± 0.18[6]
15	CH_3^+	14.8 ± 0.2	
29	$C_2H_5^+/HSi^+/CHO^+$	15.0 ± 0.2	
45	$C_2H_5O^+/C_3H_9^+/SiHO^+/CH_5Si^+$	16.4 ± 0.2	
75	$C_2H_7SiO^+/C_3H_{11}Si^+/C_4H_{11}O^+$	16.4 ± 0.2	
58	$C_4H_{10}^+/CH_2SiO^+/C_2H_8Si^+/C_3H_8O^+$	18 ± 0.5	
43	$C_2H_3O^+/C_3H_7^+/CH_3Si^+$	19 ± 0.5	
44	$C_2H_4O^+/C_3H_8^+/SiO^+/CH_4Si^+$	20 ± 1	

[a] This value is greatly affected by experimental smearing of the breakdown curves near the ionization threshold.

for acetone.[30] Hess and co-workers[6] reported the AE for *m/z* 73 from MTMSE. The latter is significantly lower (12.43 eV) than the present value of 14.4 eV. At energies below ~15 eV, the peak due to $CH_3^\bullet$ loss (MTBE, *m/z* 73; MTMSE, *m/z* 89) dominates the TOF spectra. Although this peak is the most intense peak in this region for MTBE, a second peak with *m/z* 57 corresponding to CH_3O loss is significant. The fragment ion *m/z* 43 starts to emerge above 13 eV. The MTMSE TOF spectra are completely dominated by the $CH_3^\bullet$ loss until ~13 eV where the loss of two additional methyl groups (*m/z* 59) becomes favorable, and this peak is the most intense in the mass spectra until ~30 eV. Presumably, this is loss of CH_3CH_3 to form either $SiOCH_3^+$ or CH_3SiO^+. Since the formation of either product must involve a rearrangement reaction, modeling this channel would result only in an isomerization barrier height and not new ion thermochemistry.

Methyl Loss. The threshold regions for fragmentation of the MTBE and MTMSE molecular ions occur in the energy ranges of 9.1−9.4 and 9.4−10.1 eV, respectively. The breakdown diagrams, derived from the TOF spectra, are shown in Figure 4. The breakdown curves measured at each ion source residence time were superimposible, indicating that the dissociation reactions were fast and that there was no kinetic shift in the

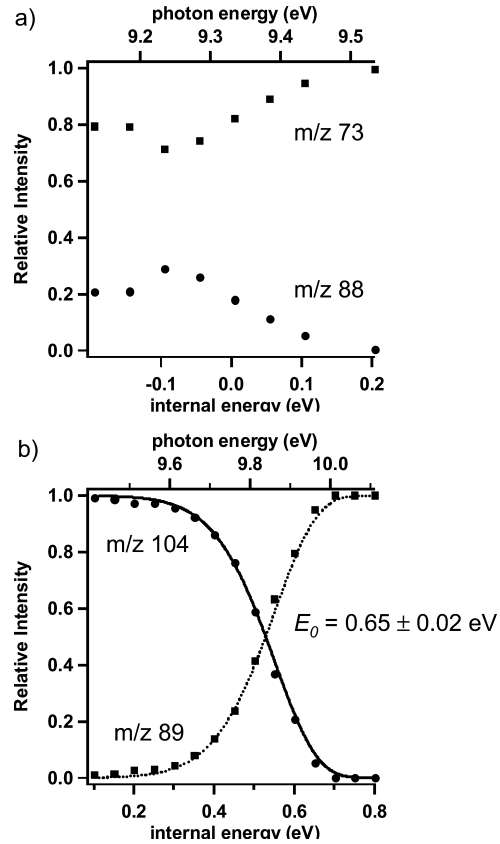

Figure 4. (a) Threshold region breakdown diagram for MTBE derived from the TOF mass spectra recorded at an ion source residence time of 1.116 μs. The G3 energy difference between neutral MTBE and the distonic ion isomer (Table 1) was used to convert from photon energy to internal energy. (b) Threshold region breakdown diagram for MTMSE derived from the TOF spectra recorded at an ion source residence time of 1.116 μs. Lines represent the RRKM fit to the experimental data.

data. For this reason, only the curves for residence times of 1.116 μs are shown in Figure 4.

In order to estimate the 0 K activation energies for the two fast processes, the $k(E)$ portion of the modeling needs simply to resemble a step function. Unfortunately, dissociation of ionized MTBE occurs over a very small internal energy window. When photon energy is converted to ion internal energy by subtracting the IE_a (either the experimental values or the G3 energy difference between neutral MTBE and the distonic isomer), all of the parent ion at *m/z* 88 disappears by an internal energy of less than 0.2 eV. In order to fit the breakdown diagrams, we need to include in the convolution the $k(E)$ step function, the internal energy distribution, and the electron transmission function. This latter function extends 0.1 eV below each measured photon energy. The result is a fit to only the two highest internal energy data points in Figure 4. Therefore, all that can be concluded from the TPEPICO data for MTBE is that the ion is only weakly bound, in agreement with the G3 relative energies (Table 1). The need to take into account the electron transmission function also precludes reading the 0 K AE for methyl loss directly from the parent ion disappearance point in the breakdown diagrams. Doing so yields an upper limit to E_0 of ~0.15 ± 0.05 eV, but this value could represent either the relative energy of ionized TBME and the dissociation products $(CH_3)_2COCH_3^+ + CH_3^\bullet$ (based on the available literature data, Table 1) or the relative energy of the distonic ion isomer and these products (based on the G3 values in Table 1).

In the modeling procedure for MTMSE, the activation energy E_0 and entropy of activation $\Delta S^{\ddagger}$ were treated as adjustable parameters and allowed to vary until a good fit was obtained between the theoretical convoluted curve and the experimental data at ion residences of 1.116, 3.116, and 5.116 μs. The fitting yielded $E_0 = 0.65 \pm 0.02$ eV/63 $\pm$ 2 kJ mol^{-1}, in excellent agreement with the G3 value of 66 kJ mol^{-1}. It was possible to vary $\Delta S^{\ddagger}$ from ~80 to 200 J K^{-1} mol^{-1} (calculated at 600 K) and obtain good fits to the experimental data due to the fact that near threshold, the dissociation rate constant curve is essentially a step function and is only dependent on the value of E_0. The best and only experimental estimate for the $\Delta_f H_{298}$ of MTMSE is -456 kJ mol^{-1}.[7] Correcting this value to 0 K (-427 kJ mol^{-1}) with the ab initio derived thermal correction and combining with the experimental IE$_a$ of 9.31 $\pm$ 0.05 eV and the above E_0 for the dissociation (63 $\pm$ 2 kJ mol^{-1}) and the $\Delta_f H_0$ for $^{\bullet}CH_3$ (150.3 $\pm$ 0.4 kJ mol^{-1})[17] leads to a $\Delta_f H_0$ for $(CH_3)_2SiOCH_3^+$ of 384 $\pm$ 10 kJ mol^{-1} ($\Delta_f H_{298} = 361 \pm 10$ kJ mol^{-1}). The above $\Delta_f H_{298}$ of MTMSE is an estimate only, and therefore, the $\pm$10 kJ mol^{-1} uncertainty associated with the $\Delta_f H$ of $(CH_3)_2SiOCH_3^+$ should be viewed as a lower limit. This value is 28 kJ mol^{-1} lower than the G3 value of 412 kJ mol^{-1} due primarily to two factors: the G3 $\Delta_f H_0$ for neutral MTMSE (-408 kJ mol^{-1}) is 16 kJ mol^{-1} higher than the value reported by Orlando et al.,[7] and the experimental IE$_a$ is 6 kJ mol^{-1} lower than the G3 estimate.

Charge Separation Reactions in Doubly Ionized MTBE and MTMSE Cations. The G3 calculations predict energies of 21.66 and 25.03 eV for the singlet and triplet states, respectively, of the doubly charged MTBE cation, while the corresponding values for MTMSE are 21.35 and 24.28 eV (relative to their respective neutrals). However, the doubly charged parent ion is not observed experimentally in either molecule, indicating that it is unstable in relation to the microsecond time scale of the measurements, and fragments into two singly charged species. Charge separation reactions of this nature were investigated in our previous study on nitrobenzene,[41] and a description was given of the procedure by which an analysis of the peak profile associated with a fragment ion could yield the initial kinetic energy possessed by that ion. This energy could then be related to the initial ion pair separation by assuming a simple Coulomb explosion model.[42] Such an analysis, which relies upon momentum conservation, is straightforward only if the fragmentation of the doubly charged parent ion results in the production of two singly charged fragments without an accompanying neutral species.

The TOF spectra for MTBE show that the width of the *m*/*z* 15 peak, associated with CH_3^+, begins to increase for photon energies above ~23 eV and that at higher excitation energies, the profile becomes a doublet, with the missing central portion being attributable to energetic fragments whose initial velocity is directed perpendicular to the TOF axis. These fragments are lost on lens apertures during their flight toward the detector. Figure 5a,b displays spectra, encompassing all of the discernible fragments, recorded at photon energies of 24 and 34 eV to illustrate the changes in the peak widths. These spectra demonstrate that a simple charge separation reaction into two stable singly charged species is not occurring. A comparison between the spectra reveals that the widths of the peaks associated with *m*/*z* 29 and 43 increase as a function of photon energy in the same way as that for *m*/*z* 15. Thus, the charge separation reaction in MTBE leads to the formation of fragment ions with *m*/*z* 15, together with either *m*/*z* 29 or 43, and their accompanying additional neutral species.

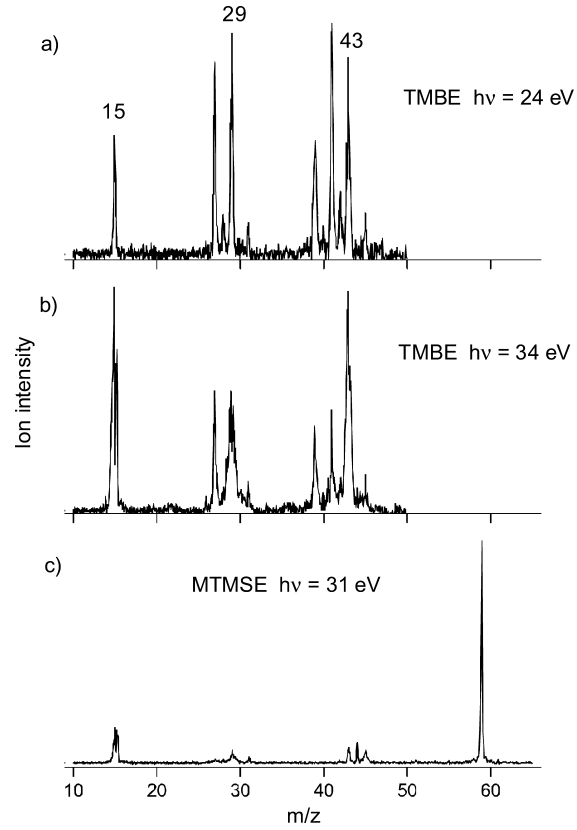

Figure 5. (a and b) TOF ion spectra of MTBE recorded at photon energies of 24 and 34 eV, respectively. (c) TOF ion spectrum of MTMSE recorded at a photon energy of 31 eV.

A similar behavior of the TOF peak widths as a function of excitation energy is observed in MTMSE (Figure 5c). At a photon energy of 31 eV, the *m*/*z* 15 peak exhibits a doublet profile, and the peaks associated with *m*/*z* 29 and 45 are broad. This increase in peak width in MTMSE occurs at the same energy, ~23 eV, as that in MTBE. Thus, in both molecules, the observed broadening occurs in the region between the calculated energies of the singlet and triplet states of the doubly charged cation.

Conclusion

Comparisons of the threshold photoelectron spectra for methyl *t*-butyl ether and methyl trimethylsilyl ether with Green's function calculations indicate that the HOMO for MTBE is a lone pair p orbital on the ether oxygen, but the same cannot be true for MTMSE. The HOMO for this molecule involves both the oxygen and *t*-butyl moiety. Kinetic modeling of the threshold region of the TPEPICO breakdown curves for the low-energy dissociation channels of MTMSE has been performed. This modeling yields 0 K activation energies of 63 kJ mol^{-1} for the dissociation of MTMSE to form $(CH_3)_2SiOCH_3^+ + {}^{\bullet}CH_3$, resulting in a $\Delta_f H_0$ for $(CH_3)_2SiOCH_3^+$ of 384 $\pm$ 10 kJ mol^{-1} ($\Delta_f H_{298} = 361 \pm 10$ kJ mol^{-1}). This value is 28 kJ mol^{-1} lower than the G3 value of 412 kJ mol^{-1} due to the G3 $\Delta_f H_0$ for neutral MTMSE (-408 kJ mol^{-1}) being 16 kJ mol^{-1} higher than the previously reported experimental value[7] and the G3 IE$_a$ being 6 kJ mol^{-1} higher. An investigation of fragment ion peak broadening at high internal energy indicated that the two doubly charged molecular ions are not stable on the microsecond time scale. Each was found to dissociate not into two singly charged fragment ions but rather into sets of two singly charged ions and one or more neutral species.

Acknowledgment. The authors are grateful to the Council for the Central Laboratory of the Research Councils (U.K.) for the allocation of beam time at the Daresbury Laboratory Synchrotron Radiation Source. P.M.M. thanks the Natural Sciences and Engineering Research Council of Canada for continuing financial support and the University of Ottawa for seed funds to undertake these experiments.

Supporting Information Available: Tables of calculated total G3 electronic energies for each species in the study, their derived G3 heats of formation, and available experimental values. This material is available free of charge via the Internet at http://pubs.acs.org.

References and Notes

(1) Di Palma, T. M.; Apicella, B.; Armenante, M.; Velotta, R.; Wang, X.; Spinelli, N. *Chem. Phys. Lett.* **2004**, *400*, 191.

(2) U.S. Environmental Protection Agency. http://www.epa.gov/mtbe/index.htm.

(3) Bhat, K. L.; Brendley, W. H., Jr.; Bock, C. W. *Soil Sediment Contam.* **2004**, *13*, 267.

(4) Bissonnette, M. C.; George, M.; Holmes, J. L. *Int. J. Mass Spectrom. Ion Process.* **1990**, *101*, 309.

(5) Beveridge, W.; Hunter, J. A.; Johnson, C. A. F.; Parker, J. E. *Org. Mass Spectrom.* **1992**, *27*, 543.

(6) Hess, G. G.; Lampe, F. W.; Sommer, L. H. *J. Am. Chem. Soc.* **1965**, *87*, 5327.

(7) Orlando, R.; Allgood, C.; Munson, B. *Int. J. Mass Spectrom. Ion Process.* **1989**, *92*, 93.

(8) Mölder, U. H.; Pikver, R. J.; Koppel, I. A. *Org. React. (N.Y. Engl. Transl.)* **1983**, *20*, 208.

(9) Sutherland, D. G.; Bancroft, G. M.; Tan, K. H. *J. Chem. Phys.* **1992**, *97*, 7918.

(10) Holland, D. M. P.; Shaw, D. A.; Sumner, I.; Hayes, M. A.; Mackie, R. A.; Wannberg, B.; Shpinkova, L. G.; Rennie, E. E.; Cooper, L.; Johnson, C. A. F.; Parker, J. E. *Nucl. Instrum. Methods* **2001**, *B179*, 436.

(11) Holland, D. M. P.; West, J. B.; MacDowell, A. A.; Munro, I. H.; Beckett, A. G. *Nucl. Instrum. Methods* **1989**, *B44*, 233.

(12) Stockbauer, R. *Int. J. Mass Spectrom. Ion Phys.* **1977**, *25*, 89.

(13) Hehre, W. J.; Radom, L.; Schleyer, P. v. R.; Pople, J. A. *Ab Initio Molecular Orbital Theory*; Wiley: New York, 1986.

(14) Frisch, M. J.; Trucks, G. W.; Schlegel, H. B.; Scusera, G. E.; Robb, M. A; Cheeseman, J. R.; Zakrzewski, V. G.; Montgomery, J. A.; Stratmann, R. E., Jr.; Burant, J. C.; Dapprich, S.; Millam, J. M.; Daniels, A. D.; Kudin, K. N.; Strain, M. C.; Farkas, O.; Tomasi, J.; Barone, V.; Cossi, M.; Cammi, R.; Mennucci, B.; Pomelli, C.; Adamo, C.; Clifford, S.; Ochterski, J.; Petersson, G. A.; Ayala, P. Y.; Cui, Q.; Morokuma, K.; Malick, D. K.; Rabuck, A. D.; Raghavachari, K.; Foresman, J. B.; Cioslowski, J.; Ortiz, J. V.; Baboul, A. G.; Stefanov, B. B.; Liu, G.; Liashenko, A.; Piskorz, P.; Komaromi, I.; Gomperts, R.; Martin, R. L.; Fox, D. J.; Keith, T.; Al-Laham, M. A.; Peng, C. Y.; Nanayakkara, A.; Gonzalez, C.; Challacombe, M.; Gill, P. M. W.; Johnson, B.; Chen, W.; Wong, M. W.; Andres, J. L.; Gonzalez, C.; Head-Gordon, M.; Replogle, E. S.; Pople, J. A. *Gaussian 98*, revision A.6; Gaussian, Inc.: Pittsburgh, PA, 1998.

(15) Scott, A. P.; Radom, L. *J. Phys. Chem.* **1996**, *100*, 16502.

(16) Curtiss, L. A.; Raghavachari, K.; Refern, P. C.; Rassolov, V.; Pople, J. A. *J. Chem. Phys.* **1998**, *109*, 7764.

(17) *NIST Chemistry Webbook, NIST Standard Reference Database Number 69*; National Institute of Standards and Technology: Gaithersburg, MD, 2000; Accessed Jan. 2009.

(18) Lias, S. G.; Bartmess, J. E.; Liebman, J. F.; Holmes, J. L.; Levin, R. D.; Mallard, W. G. *J. Phys. Chem. Ref. Data* **1988**, (Suppl.1), 17.

(19) Nicolaides, A.; Rauk, A.; Glukhovtsev, M. N.; Radom, L. *J. Phys. Chem.* **1996**, *100*, 17460.

(20) von Niessen, W.; Schirmer, J.; Cederbaum, L. S. *Comput. Phys. Rep.* **1984**, *1*, 57.

(21) Guest, M. F.; Lenthe, J. H. v.; Kendrick, J. ; Schoffel, K.; Sherwood, P. *Users Guide and Reference Manual*, version 7; Computing for Science Ltd., CCLRC Daresbury Laboratory: Cheshire, U.K., 2005.

(22) Guest, M. F.; Thomas, J. M. H.; Sherwood, P.; Bush, I. J.; Dam, H. J. J. v.; Lenthe, J. H. v.; Havenith, R. W. A.; Kendrick, J. *Mol. Phys.* **2005**, *103*, 719.

(23) Dunning, T. H. *J. Chem. Phys.* **1989**, *90*, 1007.

(24) Wilson, A. K.; Woon, D. E.; Peterson, K. A.; Dunning, T. H. *J. Chem. Phys.* **1999**, *110*, 7667.

(25) Woon, D. E.; Dunning, T. H. *J. Chem. Phys.* **1993**, *98*, 1358.

(26) Woon, D. E.; Dunning, T. H. *J. Chem. Phys.* **1994**, *100*, 2975.

(27) Baer, T.; Hase, W. L. *Unimolecular Reaction Dynamics, Theory and Experiments*; Oxford University Press: New York, 1996.

(28) Baer, T.; Mayer, P. M. *J. Am. Soc. Mass Spectrom.* **1997**, *8*, 103.

(29) Beyer, T.; Swinehart, D. R. *ACM Commun.* **1973**, *16*, 379.

(30) Rennie, E. E.; Boulanger, A.-M.; Mayer, P. M.; Holland, D. M. P.; Shaw, D. A.; Cooper, L.; Shpinkova, L. G. *J. Phys. Chem. A.* **2006**, *110*, 8663.

(31) Boulanger, A. M.; Rennie, E. E.; Holland, D. M. P.; Shaw, D. A.; Mayer, P. M. *J. Phys. Chem. A* **2008**, *112*, 866.

(32) Boulanger, A.-M.; Rennie, E. E.; Holland, D. M. P.; Shaw, D. A.; Mayer, P. M. *J. Phys. Chem. A* **2007**, *111*, 5388.

(33) Cederbaum, L. S.; Domcke, W.; Schirmer, J.; Niessen, W. v. *Adv. Chem. Phys.* **1986**, *65*, 115.

(34) Chambreau, S. D.; Zhang, J.; Traeger, J. C.; Morton, T. H. *Int. J. Mass Spectrom.* **2000**, *199*, 17.

(35) Aue, D. H.; Bowers, M. T. Stabilities of Positive Ions from Equilibrium Gas-Phase Basicity Measurements, In *Gas Phase Ion Chemistry*; Bowers, M. T., Ed.; Academic Press: New York, 1979; Vol. 2; p 1.

(36) Benoit, F. M.; Harrison, A. G. *J. Am. Chem. Soc.* **1977**, *99*, 3980.

(37) Boulanger, A.-M.; Rennie, E. E.; Mayer, P. M.; Holland, D. M. P.; Shaw, D. A. *J. Phys. Chem. A* **2006**, *110*, 8563.

(38) Rennie, E. E.; Cooper, L.; Johnson, C. A. F.; Parker, J. E.; Mackie, R. A.; Shpinkova, L. G.; Holland, D. M. P.; Shaw, D. A.; Hayes, M. A. *Chem. Phys.* **2001**, *263*, 149.

(39) Cooper, L.; Shpinkova, L. G.; Holland, D. M. P.; Shaw, D. A. *Chem. Phys.* **2001**, *270*, 363.

(40) Mackie, R. A.; Shpinkova, L. G.; Holland, D. M. P.; Shaw, D. A. *Chem. Phys.* **2003**, *288*, 211.

(41) Cooper, L.; Shpinkova, L. G.; Rennie, E. E.; Holland, D. M. P.; Shaw, D. A. *Int. J. Mass Spectrom.* **2001**, *207*, 223.

(42) Codling, K.; Frasinski, L. J. *Contemp. Phys.* **1994**, *35*, 243.

(43) Lossing, F. P. *J. Am. Chem. Soc.* **1977**, *99*, 7526.

JP900991P